Postprint of: Jerzy Hoja, Grzegorz Lentka, An analysis of a measurement probe for a high impedance spectroscopy analyzer, Measurement, Vol. 41, Iss. 1 (2008), pp. 65-75, DOI: 10.1016/j.measurement.2006.11.023

An analysis of a measurement probe for a high impedance spectroscopy analyzer

A probe for a high impedance analyzer

Jerzy Hoja, Grzegorz Lentka

Department of Metrology and Electronic Systems, Faculty of Electronics, Telecommunications and Informatics, Gdansk University of Technology,

ul. Narutowicza 11/12, 80-952 Gdansk, Poland

E-mail: hoja@eti.pg.gda.pl, lentka@eti.pg.gda.pl

Abstract. The paper presents a measurement probe which forms the input circuitry of an analyzer for high impedance spectroscopy. The probe allows measurements of impedance which is grounded at one terminal in the range of 100 Ω<$|Z_m|$≤100 GΩ. It extracts two signals proportional to current through and voltage across the measured impedance in a wide frequency range from 100 μHz up to 100 kHz. An analysis of the probe has been performed taking into account the most important parameters affecting the accuracy of the impedance measurement: parasitic capacitance at the probe input, the parameters of the transfer function of the amplifier and the tolerance of the resistors in the differential amplifier of the current signal. The formula for determining the measured impedance was elaborated, taking into consideration corrections minimizing the influence of the parasitic capacitance and the real-life parameters of the operational amplifiers.

Keywords: impedance measurement, impedance spectroscopy, high impedance measurement probe

1. Introduction

For many years, impedance spectroscopy (IS) is one of basic research methods for objects which can be modelled by an equivalent electrical circuit (e.g. electrochemistry [1], ceramic engineering [2], geology [3], buildings [4] or medicine and biology [5]). IS is very important in the case of diagnostics of anticorrosion coatings performed either in the laboratory on test samples or on the objects directly in the field (e.g. on bridges, pipelines etc.) [6, 7]. Modern anticorrosion coatings, which are achieving very high impedances Z_m>1 GΩ, create serious measurement problems. In order to identify the parameters of tested coatings it is necessary to measure impedance in a wide frequency range starting from very low frequencies of the order of 100 μHz up to 100 kHz. Additional difficulties arise due to grounding of the steel construction to be protected by anticorrosion coating (e.g. a steel railway bridge). In this case, the measured impedance of the coating is asymmetric in relation to the measurement ground, making the elimination of the influence of the parasitic capacitance of the input circuitry of the analyzer and shielded cables connecting the measurement cell difficult.

Taking into account the above conditions and the existing need of portable spectroscopy instrumentation which allows measurement directly in the field (e.g. continuous monitoring of the performance of the anticorrosion coating), the authors, using previous experiences in the construction of the laboratory impedance measurement systems [8-11], have developed an analyzer for high impedance spectroscopy of anticorrosion coatings. The accuracy of the analyzer is dependent upon the input circuit as well as on the method of determining the orthogonal parts of

measurement signals. The estimation of the accuracy of the complete measurement path is complicated and very wide. Because in case of high impedance measurements (up to 100 GΩ), the influence of the input circuitry on the measurement error is the highest, the paper is focused on the analysis of the input circuitry.

The paper is aimed to show limitations arising from real-life parameters of the input circuit and their influence on the accuracy of the impedance measurement. The analysis of parameters of input circuitry has allowed determining the formula correcting the measurement result. The formula was implemented in the built analyzer and has allowed to increase accuracy and the highest frequency of impedance measurement.

2. The architecture of the analyzer

The presented requirements concerning high impedance measurements at very low frequencies have forced the use of solutions which are not present in conventional instrumentation for impedance measurement. This applies especially to the phase-sensitive detection technique, which in traditional solutions uses multiplying circuits and mean-value circuits. For frequencies below 1 Hz, the required time constants of integrators in the phase-sensitive detectors increase from few seconds to few thousands of seconds and make this construction unusable. The developed analyzer uses a phase-sensitive detector based on Discrete Fourier Transform (DFT) for the determination of orthogonal parts (Re (·) and Im (·)) of the measurement signals, on the basis of collected sets of samples of each signal. The use of digital signal processing technique allows to determine orthogonal parts at very low frequencies starting from 100 μHz.

The need for the measurement of very high impedances has excluded the possibility of connecting the typical coating impedance (Z_x) to the input of the analyzer via

shielded cables of typical length. Because of this, the authors have decided to use a measurement probe which allows direct connection of the measured object to the input circuitry, thus eliminating to minimum the influence of parasitic capacitances on the unknown impedance Z_x. The probe extracts two signals proportional to current through and voltage across the measured impedance, which allow to determine the impedance on the basis of the definition. Two methods of current extraction are known: using a current-to-voltage converter (IUC) based on an operational amplifier [12, 13] and a series reference resistor connected to the measured impedance [14].

The method using an IUC was used in the probe presented in figure 1 [13]. The advantage of this solution is elimination of the influence of capacitance of shielded cables connecting the measured impedance of the coating to the input terminals of the probe. There is one limitation of the usage of the IUC, because it allows to measure the impedance of the anticorrosion coating only on the object which are not grounded (e.g. for coating tests in laboratory conditions).

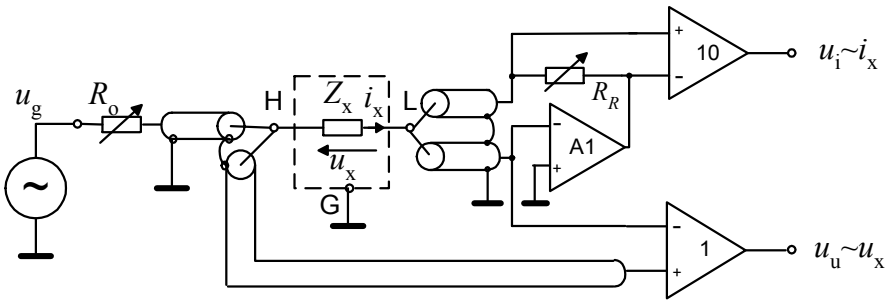

Figure 1. The measurement probe based on IUC converter.

In case of the measurement of the coating impedance on object directly in the field (and the probe is designed for such kind of measurements), the measured impedance is grounded at one terminal. In this case the use of IUC based probe is not possible and the only solution is the use of the second method (using a series reference resistor connected to the measured impedance). In this method, one of the possible ways of

elimination of the influence of capacitance of shielded cables is the use of the special doubly-shielded (triaxial) cables – internal shield with controlled potential [15]. The disadvantage of such a solution is stability which can be difficult to obtain in a wide range of measurement frequencies especially in difficult conditions, when measuring directly in the field.

Due to this fact, the authors have proposed a solution of the probe without active shielding, placed near the object under test (short cables – low capacitance) and software correction eliminating the influence of the parasitic capacitance of the shielded cables, capacitance of the inputs of operational amplifiers and layout capacitance.

2.1. The idea of the analyzer

Figure 2 presents the architecture of the realized analyzer. The object under measurement is connected to the input probe, to which the signal u_g is applied. The analyzer consists of the measurement signal u_g generation path and two identical processing paths which process measurement signals u_i and u_u extracted in the probe. The signal generation path produces a sinusoidal wave, using direct digital synthesis method (DDS), with programmable frequency, amplitude and DC offset. The signals u_i and u_u processing paths use D/A converters eliminating DC offsets, antyaliasing (low-pass) filters and fast A/D converters.

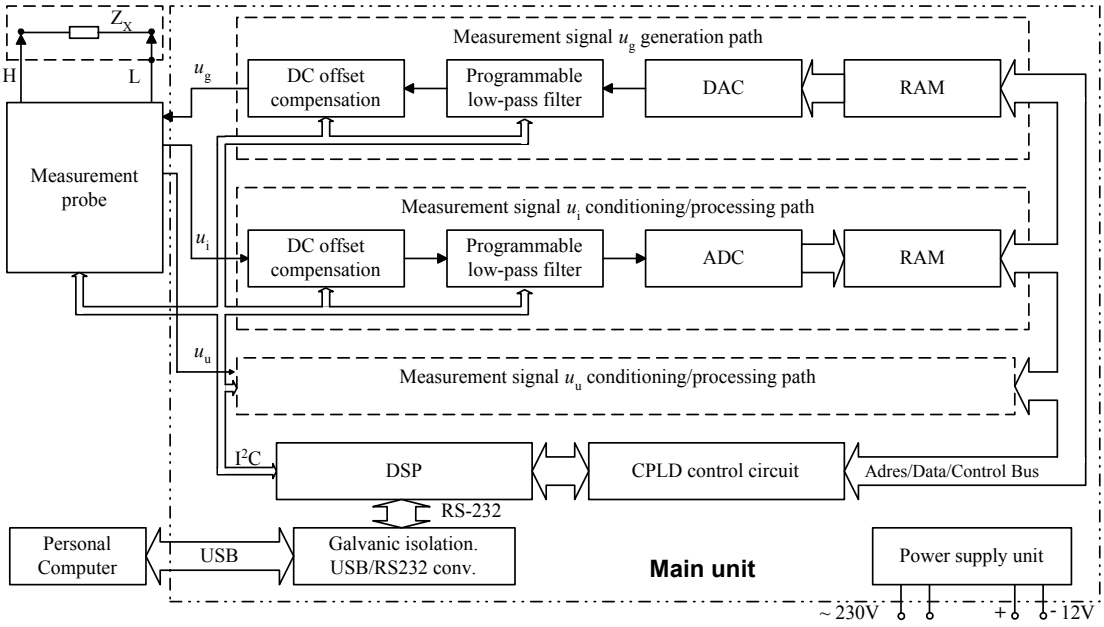

Figure 2. Block diagram of the analyzer for high impedance spectroscopy.

On the basis of two sets of samples of voltages u_i and u_u stored in RAM memories, the orthogonal parts of measurement signals are determined using DFT [16]. To assure that the obtained spectrum of each signal u_u and u_i contains only a single line, the responding measurement frequency (there is no spectral leakage), the signal samples are collected in an integer number (l) of measurement signal periods.

$$N \cdot T_s = l \cdot T \,, \tag{1}$$

where: T – measurement signal period,

$T_s=1/f_s$ f_s – sampling frequency (6.5536MHz, 655.36kHz, 65.536kHz...)

l – integer number (1-10000),

N=65536 - number of collected samples

The above condition was fulfilled thanks to the generation of the perturbation signal u_g using DDS. The generation of the sinusoidal signal is realized by approximation, using a stair-stepped wave (65536 samples in RAM) produced by a 12-bit DAC. The strobing frequency of the DAC, as well as the sampling frequency of the ADC, are selected to be

a multiple of the number of collected samples. These frequencies are obtained from 6.5536MHz reference frequency by the aid of frequency dividers realized in CPLD. Thanks to this, during generation and sampling the integer number (l) of periods of the measurement signal is always acquired in the collected number of samples (N). DFT was calculated using the definition, because the only value of a single line (l) is calculated, and the RAM memory of the DDS generator contains table of sine (cosine) values. As a result, real and imaginary part of each signal U_u, U_i can be determined as the multiplication of a series of signal samples with a series of cosine or sine samples. The calculations are made by DSP at the end of each measurement cycle. The DSP also calculates the modulus and argument of the measured impedance Z_m on the basis of formula:

$$|Z_m| = 10R_R\left|\frac{U_u}{U_i}\right|, \qquad \arg(Z_m) = \arg\frac{U_u}{U_i}. \tag{2}$$

2.2. The construction of the measurement probe

Figure 3a presents the view of the input probe connected to the measurement cell used to measure impedance of the anticorrosion coating on the railway bridge. Figure 3b presents the details of montage of measurement cell on the surface of anticorrosion coating.

a) 

b) 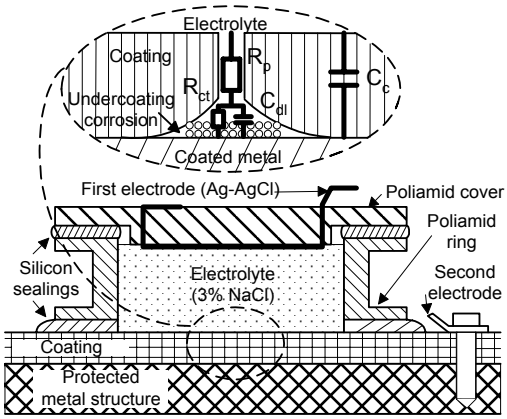

Figure 3. Input probe connected to the measurement cell (a) and the way of connecting the probe to anticorrosion coating (first electrode – terminal H, second electrode – terminal L) (b).

The developed probe allows impedance measurement of anticorrosion coatings on objects which are grounded. The probe extracts two signals proportional to current through $u_i \sim i_x$ and voltage $u_u \sim u_x$ across the unknown impedance Z_x (figure 4). The range resistor R_R connected in series with Z_x is used for the measurement of the current i_x flowing through Z_x. To assure a possibly wide measurement range of unknown impedance Z_x (the current i_x measurement range changes from 10 pA to 1 mA), range resistors R_R (100 Ω ... 100 MΩ, 1 GΩ) have been used, switched by miniature reed relays. The value of the range resistor R_R is selected in relation to $|Z_x|$ of the measured coating to assure the criterion: $0.01|Z_x| < R_R \leq 0.1|Z_x|$. When this condition is fulfilled, the resistance R_R is at least by an order lower than $|Z_x|$ and causes at least a tenfold decrease of the impedance which is seen from terminal H with respect to the ground. This situation is favourable for the sake of the decrease of noise appearing on Z_x, but causes the necessity of additional amplification 10 times of the signal from resistor R_R. This way, the amplitude of the signal u_i is comparable with respect to signal u_u, taken from the unknown impedance Z_x with the aid of the voltage follower A1.

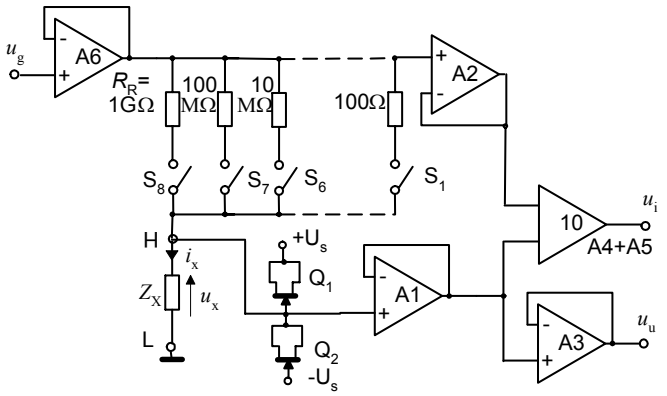

Figure 4. Schematic diagram of high impedance probe.

Because of the maximal value of the unknown impedance $|Z_x|$ = 100 GΩ, the amplifier A1 must have small input currents (on the level of a few pA) and high differential and common input impedance (Z_d, Z_c) assuming a possibly wide frequency bandwidth. Because of this, in the realized probe, the OPA627 amplifier has been used, the input currents of which do not exceed 1-2 pA (at 20 °C), and impedances Z_d and Z_c are determined by resistances $R_d = R_c$ = 10 TΩ and capacitances C_d = 8 pF and C_c = 7 pF. In order to protect amplifier A1 from overvoltages which can appear across the measured object, FET transistors (2N4117A) have been used acting as diodes with very low leakage current (<1 pA).

3. An accuracy analysis of the high impedance probe

To analyze the influence of the real-life parameters of used operational amplifiers [17] and parasitic capacitances on the extracted signals u_i and u_u, the equivalent circuit of the probe is proposed and presented in figure 5.

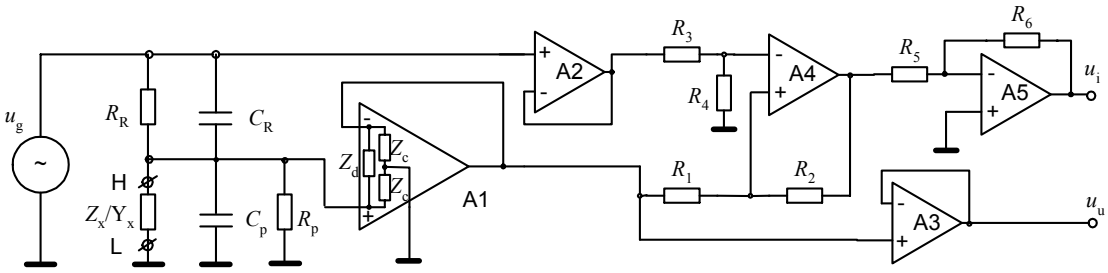

Figure 5. Equivalent circuit of the probe.

The following components have been taken into account:

$Z_R = \dfrac{1}{\dfrac{1}{R_R} + j\omega C_R}$ - impedance containing the parallel connection of range resistor R_R and capacitance C_R resulting from reed relays used to change the measurement range and range resistors R_R and layout capacitances,

C_p –capacitance resulting from shielded cables connecting the unknown impedance Z_x to the probe, transistors Q_1 and Q_2 protecting the voltage follower A1 and layout capacitances inside the probe,

R_p – leakage resistance of H terminal to the ground (e.g. leakage of the PCB laminate),

$Z_d = \dfrac{1}{\dfrac{1}{R_d} + j\omega C_d}$, $Z_c = \dfrac{1}{\dfrac{1}{R_c} + j\omega C_c}$ - differential and common impedance of amplifier A1, which connect in parallel to Z_x,

$A_u = \dfrac{A_{DC}}{1 + j\dfrac{\omega}{\omega_{3dB}}}$ - is the single-pole (ω_{3dB}) transfer function of amplifier A5, A_{DC} – open-loop gain of amplifier A5,

Nominal values of resistors: R_1-R_5 = 1 kΩ, R_6 = 10 kΩ.

On the basis of the assumed equivalent circuit of the probe, a formula for the ratio of voltages U_u and U_i was elaborated:

$$\frac{U_u}{U_i} = -\left\{\left[\left[1 + Z_R \cdot \left(\frac{1}{Z_x} + Y\right)\right] \cdot \left(\frac{1 + \dfrac{R_2}{R_1}}{1 + \dfrac{R_3}{R_4}}\right) - \frac{R_2}{R_1}\right] \cdot \left[\frac{R_6}{R_5} \cdot \frac{1}{1 + \dfrac{1}{A_u}\left(1 + \dfrac{R_6}{R_5}\right)}\right]\right\}^{-1} \tag{3}$$

where: $Y = \dfrac{1}{R_p} + \dfrac{1}{R_d} + \dfrac{1}{R_c} + j\omega\left(C_p + C_d + C_c\right)$,

It was assumed that the gain of the voltage followers A1 A2 and A3 is exactly 1 in the analyzed frequency range. The assumption is a result of fulfillment of two conditions:

- open-loop maximal frequency of the operational amplifier is a few dozen times greater than the maximal measurement frequency,
- the voltage followers are built using identical amplifiers and the ratio of signals in two paths is calculated, so gain error compensation takes place.

An analysis of the influence of real-life components of the probe on the error of impedance Z_m measurement (relative error of $|Z_m|$ and absolute error of argument of Z_m) was performed in Matlab. It was done in three stages, consecutively taking into consideration: the parasitic capacitance, parameters of the transfer function of the amplifier A5 and tolerance of the resistors setting the gain of the A4 amplifier.

3.1. Parasitic capacitances

Simulation has been performed for an object with impedance Z_x, consisting of resistor R_x = 1 GΩ and capacitor C_x = 100 pF connected in parallel. In the analyzed range of measurement frequencies from 0.01 Hz to 10 Hz, the real and imaginary parts of Z_x are comparable making objective evaluation of the measurement error possible. The assumed measurement conditions require a range resistance R_R = 100 MΩ. For simulation, zero tolerance resistors R_1-R_6 were assumed as well as open-loop gain of amplifiers $A_{DC} = \infty$, which causes that in calculation the gain of the amplifier A4 is exactly 1, and that of A5 exactly 10. Using (2) and (3), the errors of modulus and argument of Z_m (figure 6) as a function of the sum of parasitic capacitances $C_E = C_p + C_d + C_c$, for fixed value of C_R = 1 pF (the value is fully viable in case of realization of the range change by miniature reed relays).

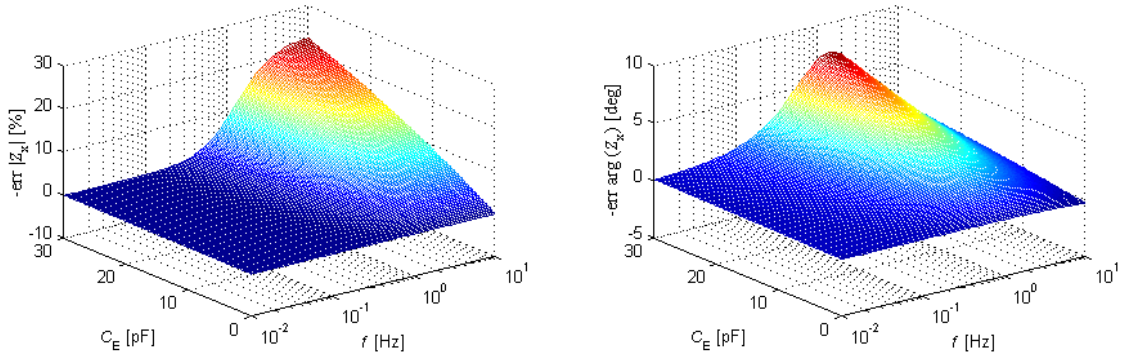

Figure 6. Relative error of modulus and absolute error of argument of Z_m as a function of parasitic capacitance and frequency.

Analyzing graphs, the significant influence of capacitance C_E on errors of the impedance parameters measurement can be noticed for frequencies higher than 0.1 Hz (for R_R = 100 MΩ). The error of the argument has the maximum value for a frequency given by the formula:

$$f_{\max(err\arg(Z_m))} = \frac{1}{2\pi R_x \sqrt{C_x\left(C_x + C_E\right)}} \ . \tag{4}$$

Because decreasing the capacitance C_E below 25 pF is difficult to realize in practice, the only way to lower the measurement error is putting the real-life value of the equivalent parasitic capacitance in the formula for determining parameters of the measured impedance.

When simulating changes of the capacitance C_R in the range of a few pF there was no significant influence on errors.

3.2. Parameters of the transfer function of the operational amplifier

In the second stage, the influence of the open-loop gain A_{DC} and the frequency f_{3dB} of the corner of the amplitude-phase characteristic of the operational amplifiers [17] used in the probe has been analyzed. Simulations were performed for the object presented in section 3.1, in the higher (10-100 kHz) measurement frequency range of the probe,

where the influence of these parameters is the highest. The optimal range resistor R_R = 1 kΩ and zero tolerance resistors R_1-R_6 were selected.

For the amplifiers working with the unity gain (A1-A4), realized with OPA627 amplifiers (A_{DC} = 120 dB, f_{3dB} = 20 Hz), the influence of A_{DC} and f_{3dB} parameters on the error can be omitted. But in case of amplifier A5 with the gain equal to 10, the use of OPA627 causes that the impedance argument error reaches a value of ca. 4° at 100kHz. Because of this, the AD817 amplifier was used in the probe ($A_{DC} = 5 * 10^3$, f_{3dB} = 10 kHz, the gain-bandwidth product $f_{3dB} * A_{DC} = 5 * 10^7$ Hz). In this case, the error of argument of Z_m does not exceed 2° and the error of modulus 0.25%, respectively.

Although the influence of the real-life amplitude-phase characteristic of A5 gain on the measurement error is much lower (with respect to the influence of the parasitic capacitance C_E), it is necessary to take it into consideration while using the formula for the determination of parameters of the measured impedance.

3.3. The resistors tolerance

The third stage includes an analysis of the influence of the tolerance of the resistors setting the gain of differential amplifier A4 on the impedance measurement error (for OPA627 amplifier, CMRR > 80 dB at 100 kHz, so its influence on the total gain can be omitted). The calculations have been performed for the range resistor R_R = 100 MΩ (R_x = 1 GΩ, C_x = 100 pF) and the R_1 and R_2 resistors tolerance changing in the range ±1%. The ratio R_2/R_1 = 1.02 means that R_2 has maximum value and R_1 has minimum value, and the ratio 0.98 presents a reverse situation (figure 7).

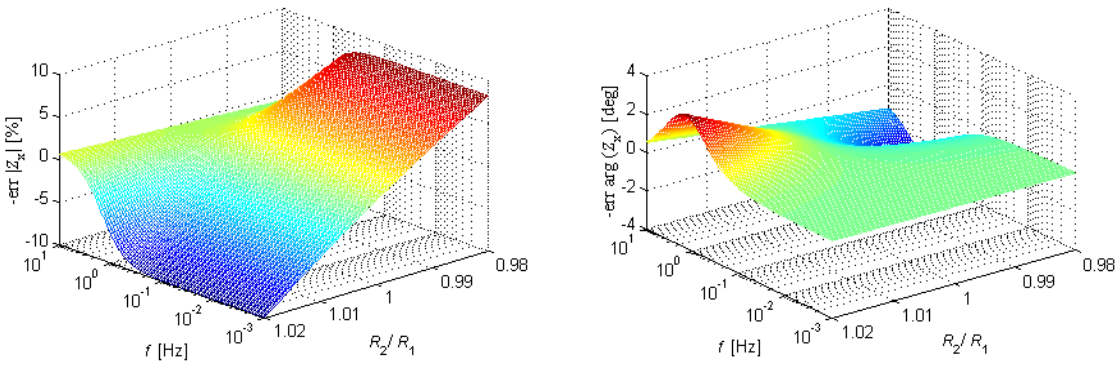

Figure 7. Relative error of modulus and absolute error of argument of Z_m as a function of tolerance of resistors R_1 and R_2 (or respectively R_3 and R_4) and frequency.

The measurement frequency, for which the greatest error appears, is dependant on two ratios: between orthogonal parts of the measured impedance ReZ_m and ImZ_m and between the impedance modulus $|Z_m|$ and range resistance R_R. These ratios decide on the phase shift between signals applied to differential amplifier and on the ratio of differential signal (signal across the range resistor R_R) and common signal (the mean value of the generator voltage u_g and voltage u_x across Z_x). In case of the measurement frequency equal to 1 Hz, parts ReZ_m and ImZ_m are comparable and a rather high common signal exists (the common signal is 3 times greater then differential one). This is a very difficult measurement condition, which decided about the great influence of resistors tolerance on impedance modulus error as well as on impedance argument error. For frequencies greater than 1 Hz, the common signal is comparable to the differential one so the errors are lower. For frequencies lower than 1 Hz the common signal is 10 times greater than the differential one, so the impedance modulus error for resistors tolerance ±1% increases up to ±10%. The impedance argument error is slightly dependent on resistors tolerance, because in this frequency range in the impedance Z_x the real part is dominating. There is no phase shift between subtracted signals and the

scalar subtraction error is close to zero. Analogous error curves were obtained when taking into consideration the R_3 and R_4 resistor tolerances.

The main conclusion resulting from performed simulations is the necessity of the use in the differential amplifier A4 resistors with much better accuracy than assumed in the analysis (1%). The resistors with ±0.01% tolerance and 5ppm temperature coefficient were used allowing accuracy on the impedance measurement error for modulus 0.1% and for argument 0.05°.

3.4. Correction of the measurement results

The use of (2) for the calculation of the parameters of the measured impedance is correct under the condition that signals u_i and u_u extracted in the measurement probe and then processed to a digital form in the main unit of the analyzer are dependent only on current i_x through and voltage u_x across Z_x. The performed analysis of the probe shows that signals u_i and u_u are also dependent on unwanted parameters (like layout capacitances, real-life parameters of operational amplifiers) causing impedance measurement errors. Because of this there is a need of using corrections on the signals extracted in the probe. Using (3) which takes into consideration the influence of main unwanted sources of errors, the following formula for the calculation of impedance Z_m has been elaborated:

$$Z_m = -\left\{ \frac{1}{10 \cdot Z_R} \cdot \frac{1 + \dfrac{11}{A_u}}{\mathrm{Re}\left(\dfrac{U_u}{U_i}\right) + j\,\mathrm{Im}\left(\dfrac{U_u}{U_i}\right)} + Y \right\}^{-1} \tag{5}$$

The formula allows to determine parameters of the measured impedance with greater accuracy. Section 4 presents the benefits obtained by using (5) for the calculation of the modulus and argument of the measured impedance of a two-terminal RC network.

4. Experimental results and discussion

In order to verify the results of simulation, measurements were performed using the realized probe and high impedance analyzer. The object connected to the probe input terminals was the reference four-element two-terminal RC network shown in figure 8. The object configuration and the component values are a typical example of the equivalent circuit of the impedance of real-life anticorrosion coatings at an early stage of exploitation.

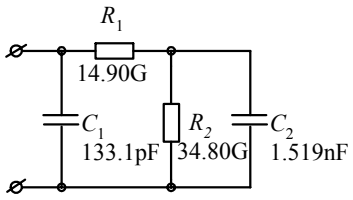

Figure 8. Electrical schematic of the reference two-terminal RC network

The capacitors of the two-terminal network were measured with a HP4192 impedance analyzer with an error not exceeding 0.1%. The two-terminal network resistors were built using resistors with nominal value of 5GΩ, which were measured using a technical method using a reference resistor 10 MΩ ± 0.01% and a HP34401A multimeter.

Ten measurement series of the two-terminal network impedance were performed for frequencies in range 100 kHz–100 μHz (with 1-2-5 steps), with an amplitude of the measurement signal of 1 V_{RMS}. The calculated mean values of the obtained results of modulus and argument of impedance are shown in figure 9 (no correction was applied).

For each measurement points the standard deviation of the impedance modulus does not exceed 0.5% and for argument of impedance is lower than 0.25°.

Figure 9 also shows the modulus and argument characteristic of the tested two-terminal network calculated theoretically on the basis of the reference RC components.

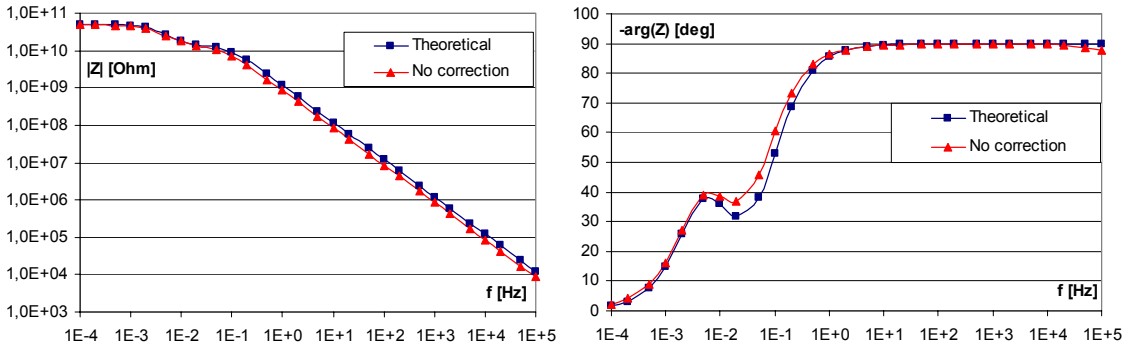

Figure 9. The modulus and argument of impedance of the tested two-terminal RC network

When comparing the presented graphs a shift of the impedance modulus curve can be noticed. It is caused by the parasitic capacitance C_E. This capacitance also causes that the argument curves differ in the frequency range 0.01 Hz-1 Hz, because in this range the Re(.) and Im(.) parts of the two-terminal network impedance are on a similar level. Below this range (<0.001 Hz) the real part dominates, but above the range (>1 Hz) the capacitive part is dominating. In the impedance argument graph for frequencies above 10 kHz the influence of the phase shift entered by amplifier A5 can be seen.

The impedance spectroscopy curves of the two-terminal RC network presented in figure 9 have significant changes in modulus (10 kΩ-50 GΩ) and argument (90 °-2 °) of impedance, thus making a precise evaluation of the influence of the analyzed parameters on the accuracy of the measurement impossible. Because of this, the impedance spectrum calculated theoretically was assumed to be real and the relative

errors of modulus and the absolute errors of argument of impedance have been calculated taking into account main parameters of the probe.

In figure 10, errors for four different values of parasitic capacitances C_E have been presented: for the measured capacitance $C_E^m = 54$ pF (explained in next part of section) and for values decreased by 10 pF and 5 pF and increased by 2 pF with respect to C_E^m.

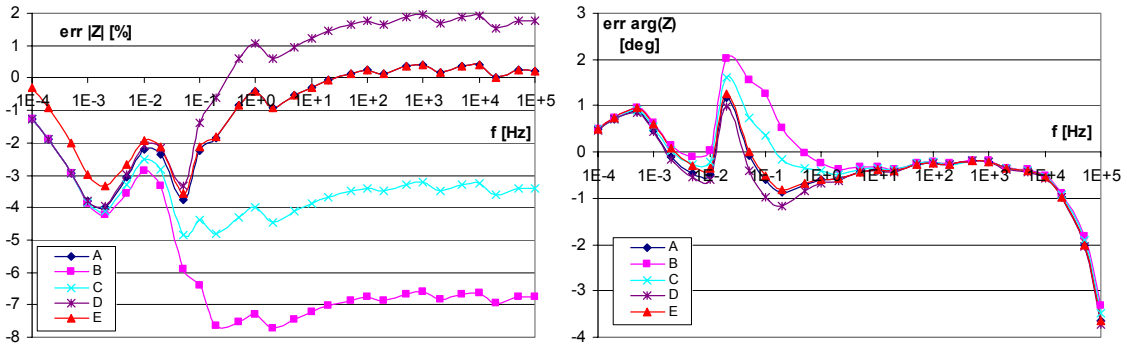

Figure 10. Error of modulus and argument of impedance of two-terminal RC network for different degrees of compensation of the parasitic capacitance C_E

A - C_E^m, B - C_E^m - 10 pF, C - C_E^m - 5 pF, D - C_E^m + 2 pF, E - C_E^m; $R_p = 5$ TΩ

In the graphs, it can be seen, that the modulus error is strongly dependant on parasitic capacitance for frequencies above 0.1 Hz, where the capacitive component dominates in the impedance of the two-terminal RC network, but the argument error is dependent in a narrower frequency range (0.001 Hz-0.1 Hz), where the real and the imaginary parts of the impedance of the two-terminal RC network are comparable (or one of them is slightly dominating). The four curves under analysis did not take into account the leakage resistance R_p existing in the probe. Taking this resistance ($R_p = 5$ TΩ) into account shows an influence only on the error of the impedance modulus only at frequencies below 0.01 Hz, where the resistive part dominates in the two-terminal RC network.

The error curves presented in figure 10 show that it is very important to precisely know the actual values of C_E and R_p in order to decrease errors. These parameters rely on many components: the operational amplifier used as voltage follower A1 (C_c, C_d, R_c, R_d), the protecting FET transistors, the shielded cables (ca. 20 cm long) connecting the object under the measurement, layout capacitances etc., so in order to determine these parameters the measurement was done using the FRA1255 analyzer from Solartron. To do this, the probe with open input terminals (but with connected shielded cables) was connected to the FRA1255 analyzer. The measurements of the U_u/U_i signal complex ratio were performed at two frequencies. At 1 kHz, on the basis of (2) the parasitic capacitance C_E=54pF was determined and at 1 mHz the leakage resistance R_p = 5 TΩ was found. Measured value of C_E tallies with estimated value of resultant capacitance obtained from summing its components: capacitance of the shielded cable (ca. 30pF), C_c+C_d=15pF (from datasheet of OPA627) and two FET's capacitance 2*3pF=6pF (from datasheet of 2N4117A) and layout capacitance ca. 3pF.

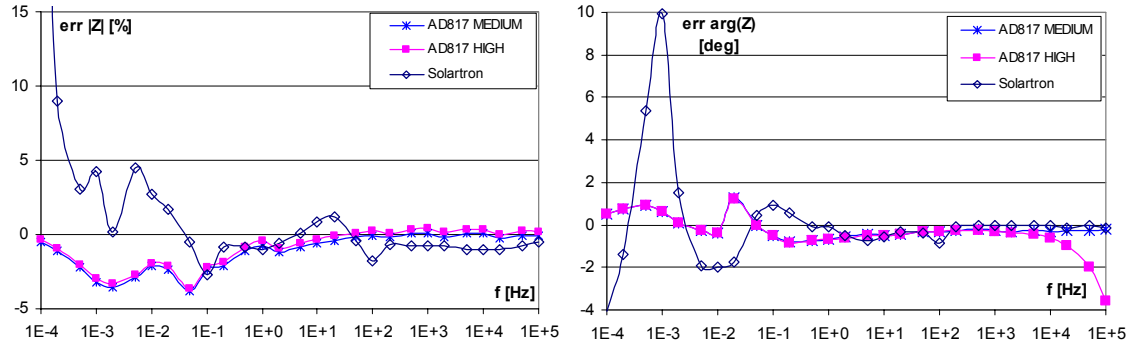

Figure 11. Measurement error of modulus and argument of two-terminal RC network for the realized analyzer (for different values of parameters of the operational amplifier A5) and for the set of Solartron instruments

Figure 11 presents errors of impedance measurement, which were determined when putting into (5) different values of parameters ω_{3dB} and A_{DC} of amplifier A5. For

calculations the parasitic capacitance C_E and leakage resistance R_p values were assumed to minimize measurement errors (C_E=54pF, R_p = 5 TΩ). When analyzing graphs it can be noticed that the influence of the above parameters is important only at measurement frequencies greater than 10 kHz. Taking into consideration that A_{DC} parameter of the amplifier AD817 can change in range 4000-6000, two cases were taken into account: 5000 (MEDIUM) and 6000 (HIGH). Watching the error curves, it can be noticed that the used amplifier has a gain of 5000, for which the impedance measurement error at 100 kHz is minimal.

In order to evaluate the realized probe, the comparative measurements of the object presented in figure 8 were performed using a set of Solartron instruments, FRA1255 and Impedance Interface 1294; the calculated errors were shown in figure 11. When applying software corrections in the realized analyzer, the curves show that the measurement error is significantly lower for the realized analyzer, especially for frequencies below 1Hz ($|Z_x|$≥1GΩ), than for the Solartron set of instruments.

Resuming, it can be said that the evaluation of the real-life measurement probe proves the presented analysis based on the proposed equivalent electrical circuit (figure 5). This leads to possibility of the use of simulations in the probe development process in order to minimize the measurement errors. The most important profit of performed analysis is development of the corrections, which were implemented in realized analyzer and improved accuracy of the impedance measurement as shown in figures 10 and 11. The developed way of entering corrections gives the user the possibility of running calibration procedure. The procedure performs automatic determination and entering capacitance of used shielded cables and measurement cells before impedance spectroscopy experiment.

5. Conclusions

The realized analyzer for high impedance spectroscopy uses the digital signal processing technique to determine orthogonal parts of measurement signals. This allows measurements in a wide frequency range from very low 100 μHz up to 100 kHz. Thanks to the use of the input circuitry in the form of a measurement probe, the analyzer makes measurement in range of 100 Ω<$|Z_m|$≤100 GΩ (in 8 subranges) possible.

The analysis of the probe has been performed making possible evaluation of the accuracy of the impedance measurement. The strong dependence of the error of the impedance modulus and argument on the parasitic capacitance at the probe input, parameters of the transfer function of the amplifier with the gain equal to 10 (in the higher frequency range >10kHz) and on the accuracy of the resistors in the differential amplifier of the current signal. The possibilities of error sources reduction have been presented (the use of precise resistors and wide bandwidth operational amplifier) and entering software corrections for error sources which cannot be reduced (parasitic capacitance and leakage resistance).

The comparison between the results of simulations and the results of measurements of the realized probe prove that the assumed equivalent circuit of the probe is correct and takes main real-life parameters of the probe into account. Due to this fact, the formula determining the signals extracted in the probe can be used to elaborate the equation for correcting the influence of the parasitic capacitance and real-life parameters of the operational amplifier. It was shown that the parameters of the measured impedance were calculated on the basis of the elaborated equation with an error of +0.5%/–3.5% in case of modulus and ±1° in case of argument in whole range of

measurement frequencies. The elaborated formula improving significantly the impedance measurement accuracy was implemented in software of the PC controlling the analyzer. The noticeable lower impedance measurement error were obtained when comparing to commercially available instruments set from Solartron, especially for frequencies lower than 1Hz ($|Z_x| \geq 1G\Omega$).

The software is capable to determine and take into calculation the actual value of the capacitance of cables used to connect measurement cell with the probe terminals. This gives the user the freedom of the use of the probe in different field conditions while assuring minimalisation of errors.

Acknowledgments

This work was founded by the Polish Ministry of Scientific Research and Information Technology, through European project Eureka E!3174. The authors would also like to acknowledge the scientific contribution and help in the testing analyzer provided by Prof. Pier Luigi Bonora and his team from Department of Materials Science and Engineering University of Trento and PhD Agnieszka Krolikowska and PhD Jacek Bordzilowski from the Roads and Bridge Research Institute from Warsaw Poland.

References

[1] H. Andersson, I. Petersson, E. Ahlberg, Modelling electrochemical impedance data for semi-bipolar lead acid batteries, J. Applied Electrochemistry 31 (2001) 1-11.

[2] K. Srinivas, P. Sarah, S. V. Suryanarayana, Impedance spectroscopy study of polycrystalline $BI_6FE_2TI_3O_{18}$, Bull. Mater. Sci. 26 (2003) 247-253.

[3] J. Xiang, N. B. Jones, D. Cheng, F. S. Schlindwein, Direct inversion of the apparent complex-resistivity spectrum, Geophysics 66 (2001) 1399-1404.

[4] R. T. Coverdale, B. J. Christensen, T. O. Mason, H. M. Jennings, E. J. Garboczi, D. P. Bentz, Interpretation of impedance spectroscopy of cement paste via computer modeling, J. Mat. Sci. 30 (1995) 712-719.

[5] S. Nebuya, B. H. Brown, R. H. Smallwood, P. Milnes, A. R. Waterworth, M. Noshiro, Measurement of high frequency electrical transfer impedances from biological tissues, Electronics Letters 35 (1999) 1985-1987.

[6] F. Deflorian, S. Rossi, L. Fedrizzi, P. Bonora, The application of electrochemical impedance spectroscopy for studying the mechanism of corrosion protection by organic coating, Proc. Of The Third International Conference on Electrochemistry ICE III Luxor, Egypt, 13-15/02/2001 1 (2001) 29-30.

[7] A. Carullo, M. Parvis, A. Vallan, Fast impedance analyzer for corrosion monitoring, Proc. of XVI IMEKO World Congress Vienna 6 **(**2000**)** 161-165.

[8] J. Hoja, G. Lentka, Virtual instrument using bilinear transformation for parameter identification of high impedance objects, Meas. Sci. Tech. 4 **(**2003**)** 633-642.

[9] J. Hoja, A metrological analysis of the input circuit of an impedance meter*,* Metrology and Measurement Systems 10 (2003) 367-380.

[10] J. Hoja, G. Lentka, The high impedance measuring probe for gain-phase analysers*,* Proc. XII International Conference on Electrical Bioimpedance & V Electrical Impedance Tomography Gdańsk (2004) 375-378.

[11] J. Hoja, G. Lentka, The influence of parameters of input probe on the error of high impedance measurement, 14th IMEKO TC4 Symposium Gdynia-Jurata Poland 1 (2005) 25-30.

[12] R. Dygas, M. W. Breiter, Measurements of large impedances in a wide temperature and frequency range, Electrochimica Acta Vol. 41 (1996) 993-1001

[13] J. Hoja, G. Lentka, New measurement probe for high impedance spectroscopy, Proc. of 2006 IEEE Instrumentation & Measurement Technology Conference - IMTC 2006, Sorrento, Italy, 24-27 April 2006, 323-328.

[14] G. Chiodelli, P. Lupotto: Experimental approach to the impedance spectroscopy technique, J. Electrochem. Soc., Vol. 138, No. 9, September 1991, 2703-2711.

[15] Solartron: High Impedance Interface 1294 Operating Manual, Dec. 2001

[16] G. Lentka, J. Hoja, The influence of sampling parameters on accuracy of capacitance measurement in the method based on DSP. Proc. 13th International Symposium on Measurements for Research and Industry Applications IMEKO TC4. Athens 2004, Vol. 1, 294-297.

[17] S. Franco, Operation amplifiers and analog integrated circuits. McGraw-Hill Book Company, 1988.

Figure captions:

Figure 1. The measurement probe based on IUC converter.

Figure 2. Block diagram of the analyzer for high impedance spectroscopy.

Figure 3. Input probe connected to the measurement cell (a) and the way of connecting the probe to anticorrosion coating (first electrode – terminal H, second electrode – terminal L) (b).

Figure 4. Schematic diagram of high impedance probe.

Figure 5. Equivalent circuit of the probe.

Figure 6. Relative error of modulus and absolute error of argument of Z_m as a function of parasitic capacitance and frequency.

Figure 7. Relative error of modulus and absolute error of argument of Z_m as a function of tolerance of resistors R_1 and R_2 (or respectively R_3 and R_4) and frequency.

Figure 8. Electrical schematic of the reference two-terminal RC network

Figure 9. The modulus and argument of impedance of the tested two-terminal RC network

Figure 10. Error of modulus and argument of impedance of two-terminal RC network for different degrees of compensation of the parasitic capacitance C_E

A - C_E^m , B - C_E^m - 10 pF, C - C_E^m - 5 pF, D - C_E^m + 2 pF, E - C_E^m ; R_p = 5 TΩ

Figure 11. Measurement error of modulus and argument of two-terminal RC network for the realized analyzer (for different values of parameters of the operational amplifier A5) and for the set of Solartron instruments